Materials Characterization 134 (2017) 96-102

Infusion of hydrogen into nanostructured bainitic steel

A. B. Cota[a,1], *S. W. Ooi*[b,2], *W. Solano-Alvarez*[b,3], *H. K. D. H. Bhadeshia*[b,4]

[a] *Department of Physics, Federal University of Ouro Preto, Ouro Preto Brazil*
[b] *Materials Science and Metallurgy, University of Cambridge, Cambridge, U.K*

[1]*abcota@ufop.br*, [2]*swo23@cam.ac.uk*, [3]*ws298@cam.ac.uk*, [4]*hkdb@cam.ac.uk*

Abstract

The trapping of hydrogen in nanostructured bainitic steel has been investigated using thermal desorption analysis, in order to determine the potency of the ferrite-retained austenite (α/γ) interfaces and retained austenite as trapping sites. Thermal desorption data showed that the volume of retained austenite is more effective in trapping hydrogen than the interfaces. There is a close correlation between the quantity of hydrogen and the retained austenite content rather than the density of interfaces. A local equilibrium model was able to reproduce the hydrogen desorption behaviour of saturated and unsaturated samples considering both retained austenite and α/γ interfaces as the trapping sites. A trap binding energy ranging from 47-52 kJ/mol was estimated for retained austenite, suggesting that the observed trapping capacity originates from the austenite lattice sites.

Keywords: hydrogen; thermal desorption analysis; nanostructured bainite; trapping energy.

Introduction

Nanostructured bainitic steels consist of thin plates of ferrite separated by films of carbon-enriched retained austenite and display an excellent combination of properties including strength and ductility [1-3]. The high strength makes them susceptible to hydrogen embrittlement that can lead to delayed fracture and a loss of structure [4-7].

It is well known [6] that it is diffusible hydrogen which embrittles, and its passage through a steel can be impeded by “traps”, where a hydrogen atom can enter a potential well that is deeper than in a perfect lattice. The traps tend to attract and bind the atomic hydrogen, and the damage is minimised if the hydrogen is immobilized [6,8,9].

The austenite volume fraction and morphology in the nanostructured bainite forms a continuous barrier between the ferrite plates, i.e. the austenite percolates through the microstructure and reduces the infusion of hydrogen [10]. Moreover, retained austenite is an effective trap given its high solubility and low diffusivity for hydrogen [10-13]. There is a high dislocation density in both phases (α,γ) at the interface due to the relaxation of the shape deformation induced by transformation. The dislocation density increases as the transformation temperature decreases [14-18], and dislocations are known to be trapping sites for hydrogen [9,19,20]. Nanostructured bainite contains a very large surface area of α/γ interfaces per unit volume due to the fine scale of the bainitic ferrite plates [1-3] and these α/γ interfaces may also act as hydrogen traps [7,20,21].

Hydrogen traps in different kinds of steel microstructures have been characterised using thermal desorption analysis (TDA). This technique allows the

investigation of hydrogen absorption and desorption mechanisms, by monitoring the rate at which it is released from a sample during continuous heating. The experiment provides valuable information for the development of new materials with a higher resistance to hydrogen embrittlement [20-22]. In a thermal desorption experiment, hydrogen evolved at a low temperature is weakly trapped whereas the strongly trapped hydrogen is only released at higher temperatures. Typical traps for hydrogen and the associated binding energies (E_b) were summarized by Szost et al.[21]. The weak hydrogen traps (reversible traps) include grain boundaries (E_b=17.2kJ/mol), dislocations (26.8kJ/mol), ferrite/Fe_3C interface (18.4kJ/mol) and microvoids (35.2kJ/mol). The strong hydrogen traps (irreversible traps) include TiC/incoherent (86.9kJ/mol), retained austenite (55kJ/mol) and Fe_3C/incoherent (84kJ/mol).

Previous studies on hydrogen in nanostructured bainite have suggested that the level of hydrogen saturation is correlated to the total area of α/γ interfaces per unit volume rather than to the volume fraction of retained austenite [7,21]. However, this result does not account for the conflicting values of retained austenite after isothermal transformation [21] or assumptions in bainitic ferrite plate width that affect the estimation of surface area per unit volume of the α/γ interfaces [7].

In order to bring new elements of understanding about hydrogen trapping in nanostructured bainitic steel, thermal desorption analysis was used to study the potency of α/γ interfaces and retained austenite as hydrogen trapping sites. The effect of hydrogen trapping at α/γ interfaces and retained austenite during TDA experiments was simulated by using one of the hydrogen desorption models developed by Song et al. [20]

Material and Experimental Procedures

The alloy selected for this work (0.78C–1.60Si–2.02Mn–1.01Cr–0.24Mo–3.87Co–1.37Al wt.%) has been designed to obtain a nanostructured carbide-free bainitic structure after isothermal heat treatment at low temperatures. A BAHR DIL805 high resolution dilatometer was used to track the isothermal decomposition of austenite into bainitic ferrite in samples 4 mm in diameter and 10 mm long, heated at 950 °C for 30 minutes and subsequently cooled at 30°C/s to the isothermal temperatures of 200 °C for 72 h, 250 °C for 16 h and 300 °C for 6 h. The experimental bainite and martensite start temperatures, B_S and M_S, are 410 °C and 188 °C, respectively [23]. Figure 1 shows the dilatometric curves during isothermal transformation and the determination of the time needed to stop the heat treatment, which was fixed at the point where the dilatometric strain achieved a steady state or plateau (i.e., no further transformation) [18].

Samples 50 mm x 20 mm x 1 mm were austenitized at 950 °C for 30 minutes, followed by isothermal transformation at 200 °C for 72 h, 250 °C for 11 h and 300 °C for 4 h, which correspond to the measured times. Vickers hardness tests are reported as the average of indentations conducted using a 193.13 N (20 kgf) load.

The volume fraction and lattice parameters of the phases present in the microstructure after the heat treatments were determined by doing Rietveld refinement of data collected using a Bruker D8 Advance diffractometer with a position sensitive detector and CuKα radiation. Scans were performed from 35 to 130°, with a step size of 0.02°, a dwell time of 3.5 s, and energy levels from 210 to 220 mV to minimize beta peaks. The samples were rotated at 30 rad/s and 10 mm slits were chosen to restrict the beam size. After scanning, the simulated slit mode was changed to fixed in order to flatten the background as much as possible. Samples were prepared by grinding with 4000 SiC paper, polishing to 1 μm, etching in 2%

nital, and polishing again to 1 μm to get rid of any surface stresses and/or stress induced austenite transformation.

Thin foil samples for transmission electron microscopy were prepared from discs 3 mm in diameter, cut using a punch. They were ground down to 50 μm in thickness and electropolished until perforation with an electrolyte of 5 % perchloric acid, 20 % glycerol and 75 % ethanol at -8°C and 22 V. The thin foils were examined using a FEI Tecnai F20 FEGTEM transmission electron microscope operated at 200 kV and the micrographs were used to determine the size of bainitic ferrite plate thickness, t_B, by measuring the mean lineal intercept $L_T = \pi t_B/2$ in a direction normal to the plate length [2,24].

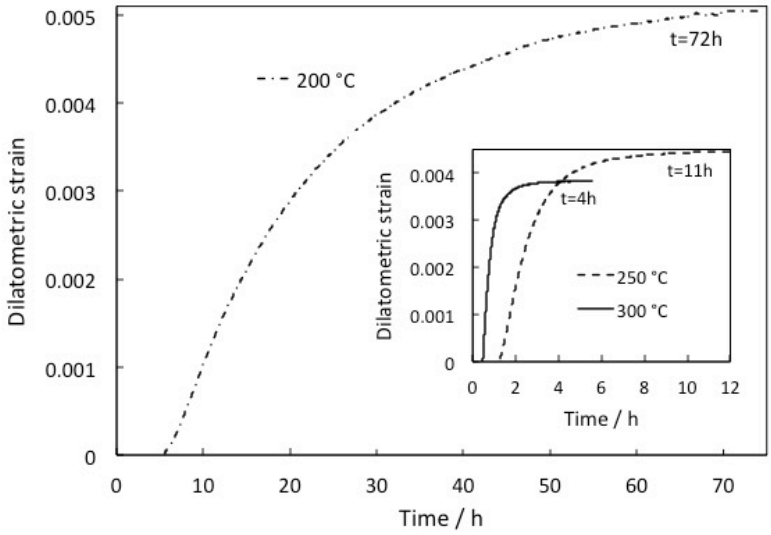

Fig. 1- Dilatometric curves showing strain associated with the bainite transformation at different transformation temperatures for estimation of the end of the bainitic transformation.

For TDA analysis, samples 50 mm x 20 mm x 1 mm were polished with the 600 SiC paper and charged electrochemically with hydrogen in a 3.5 % NaCl aqueous solution containing 0.35 % NH_4SCN with a current density of 10 A/m^2 for 4 h (unsaturated) and 48 h (saturated) at room temperature. The amount of hydrogen was measured through thermal desorption analysis during continuous heating from room temperature to 300 °C at a constant heating rate of 50 °C/h. The samples were analysed at an interval of 3 minutes using He as a carrier gas. Samples charged for 4 h and 48 h were analysed within 15 minutes after hydrogen charging. To analyse the amount of hydrogen trapped, some samples were kept at room temperature for 7 days after being charged for 48 h, before being analysed in TDA.

Results

Rietveld refinement of all the X-ray diffraction data collected was performed in HighScore Plus according to the method presented in [25] by first fitting austenite to three isolated austenite peaks: 002, 022, and 113. This allowed to obtain maximum and minimum estimates for the lattice parameter of austenite, which were then used to calculate its carbon concentration through the Dyson and Holmes equation [26]. Since this carbon concentration is inherited by martensite, its maximum and minimum values of tetragonality were obtained by using the Honda and Nishiyama

charts [27]. These lattice parameters (a_γ, $a_{\alpha'}$, and $c_{\alpha'}$) were used to fit martensite, retained austenite, and bainitic ferrite to the whole spectrum. The results suggest there is no martensite present.

X-ray diffraction patterns show, as expected from the increase in driving force as a function of undercooling, that the austenite volume fraction in the as-transformed samples decreased as the isothermal transformation temperature was reduced (Table 1). Since the carbon is not only present in solid solution in the bainitic ferrite but also located at defects such as dislocations [28,29], the concentration of carbon trapped at defects was estimated by means of residue $x_\rho = \bar{x} - V_\gamma x_\gamma - (1 - V_\gamma)x_\alpha$, where $\bar{x}$ is the average concentration of carbon in the steel, x_α and x_γ are the carbon concentration in ferrite and austenite respectively, and V_α and V_γ are the respective volume fractions. Consistent with expectation, the data indicate that the defect density increases as the transformation temperature is reduced.

Table 1. Compiled results for X-ray diffraction data. a_γ and a_α represent the lattice parameters of austenite and ferrite respectively, with a Rietveld fitting error of ≤0.001 Å. x_α and x_γ are the respective carbon concentrations (in wt. %), V_α and V_γ are the respective volume fractions, and x_ρ the is estimated concentration of carbon trapped at defects.

Transformation temperature	V_α	V_γ	a_α / Å	a_γ / Å	x_α	x_γ	x_ρ
200°C	0.79±0.01	0.21±0.01	2.8730	3.617	0.187	0.850	0.454
250°C	0.74±0.01	0.26±0.01	2.8714	3.6229	0.131	1.029	0.416
300°C	0.66±0.01	0.34±0.01	2.8682	3.6266	0.021	1.141	0.378

The microstructure consists essentially of a mixture of two phases, thin plates of bainitic ferrite and carbon enriched regions of retained austenite with morphologies of films and micro-blocks as described by other authors [30,31]. Figure 2 illustrates the microstructure obtained from TEM for the samples isothermally transformed, where the lighter phase is ferrite and the darker is retained austenite. The micrographs also show the scale of the structure with corresponding measurements shown in Table 2. The low transformation temperatures resulted in nanostructured bainite with an apparent thickness ranging from 40 to 71 nm. Decreasing plate thickness was expected as the isothermal transformation temperature decreased. In Table 2, the surface area per unit volume of the ferrite plates, S_v, which is proportional to the ratio between ferrite volume fraction (V_α) and ferrite plate thickness (t_B), $S_v=V_\alpha/t_B$, and the Vickers hardness, HV20, are also listed.

The samples charged with hydrogen for 48 h presented a reduction of hardness by about 3 % with respect to as-transformed samples (Table 2). The hardness did not change when measured one week after hydrogen charging. It is not clear why there was a small reduction in hardness after hydrogen charging, but it is speculated that damage in the form of voids or microfissures may have taken place during charging, thus contributing to softening."

Calculations using a diffusion coefficient for hydrogen in austenite, $D=3.14\times10^{-16}$ m^2/s at room temperature [32], a time of t=48 h and the equation $C_{rel}=1-\text{erf}\{x/[2(Dt)^{1/2}]\}$ indicate a penetration distance (x) of about 1 μm for a relative average concentration $C_{rel}=0.96$. This distance is greater than the half-size of retained austenite micro-blocks [18], confirming that the samples charged with hydrogen for 48 h were saturated, i.e., there is a uniform hydrogen concentration through the sample thickness.

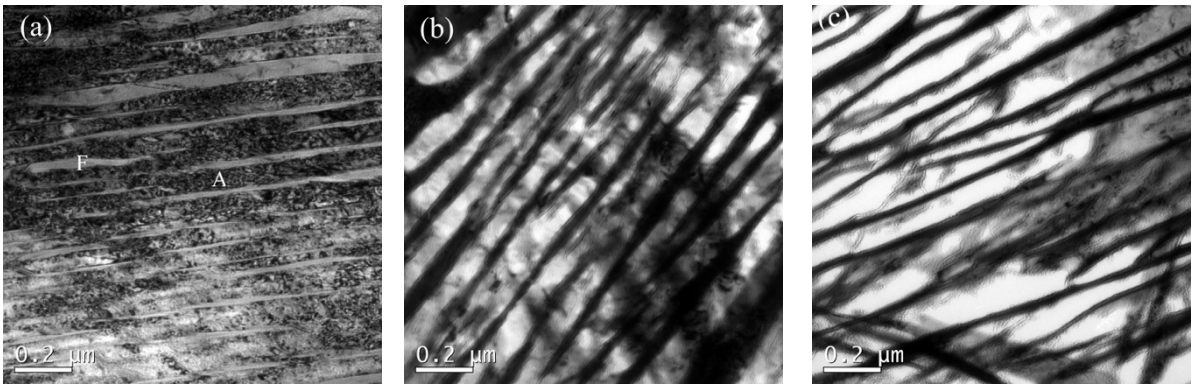

Fig. 2- TEM image (bright field) of samples transformed at (a) 200 °C/72 h, (b) 250 °C/11 h and (c) 300 °C/4 h. F – ferrite, A – austenite.

Table 2. Quantitative experimental data. The ferrite thickness, t_B, refers to the stereologically corrected value and S_V is the surface area per unit volume. HV20 is the average Vickers hardness of 70 indentations using a 196.12 N (20kgf) load and standard error with 95% confidence interval. HV20 - aHC refers to the hardness of 10 indentations after H-charging.

Transformation temperature	t_B / nm	$S_V=V_\alpha/t$ $(nm)^{-1}$	HV20	HV20 - aHC
200 °C	40±3	0.01975	660±2	645±7
250 °C	54±3	0.01370	610±2	591±5
300 °C	71±4	0.00930	520±2	503±5

Figure 3 shows the obtained TDA curves, using a heating rate of 50 °C/h and hydrogen charged samples. The peaks of the hydrogen desorption curve for samples charged for 48 h and analysed 15 minutes after H-charging (aHC) are shifted to higher temperatures as the isothermal transformation temperature increases (Figure 3a). When the isothermal transformation temperature decreased from 300 °C to 200 °C the surface area per unit volume of α/γ interfaces increased from $9.30x10^6$ to $1.98x10^7$ m^{-1}, the fraction of retained austenite decreased from 0.34 to 0.21 and the total hydrogen desorbed decreased from 17.46 to 11.27 ppmw (parts per million by weight) respectively (Table 3). A larger amount of hydrogen is stored in the retained austenite and at α/γ interfaces in the saturated condition. Each desorption curve shows a single peak (or indistinguishable overlapping peaks). The presence of retained austenite is associated clearly with the capacity to store hydrogen since its volume fraction is found to have a large effect on the total amount of absorption. The larger fraction of retained austenite resulted simultaneously in an increase in peak temperature and in the amount of hydrogen desorbed.

The peak temperatures increased when the measurement was carried out one week after H-charging (wHC), for samples charged with hydrogen for 48 h (Figure 3b). The diffusible or weakly trapped hydrogen (reversibly trapped hydrogen) was largely released (≈97-99 % of the total hydrogen absorbed) at room temperature (Table 3), but the hydrogen atoms that remain in films and micro-blocks of retained austenite were released at a high peak temperature (≈150 °C) for the three isothermal transformation temperatures. The amount of hydrogen that remained is less than 0.1 ppmw for samples isothermally transformed at 200 °C and 250 °C.

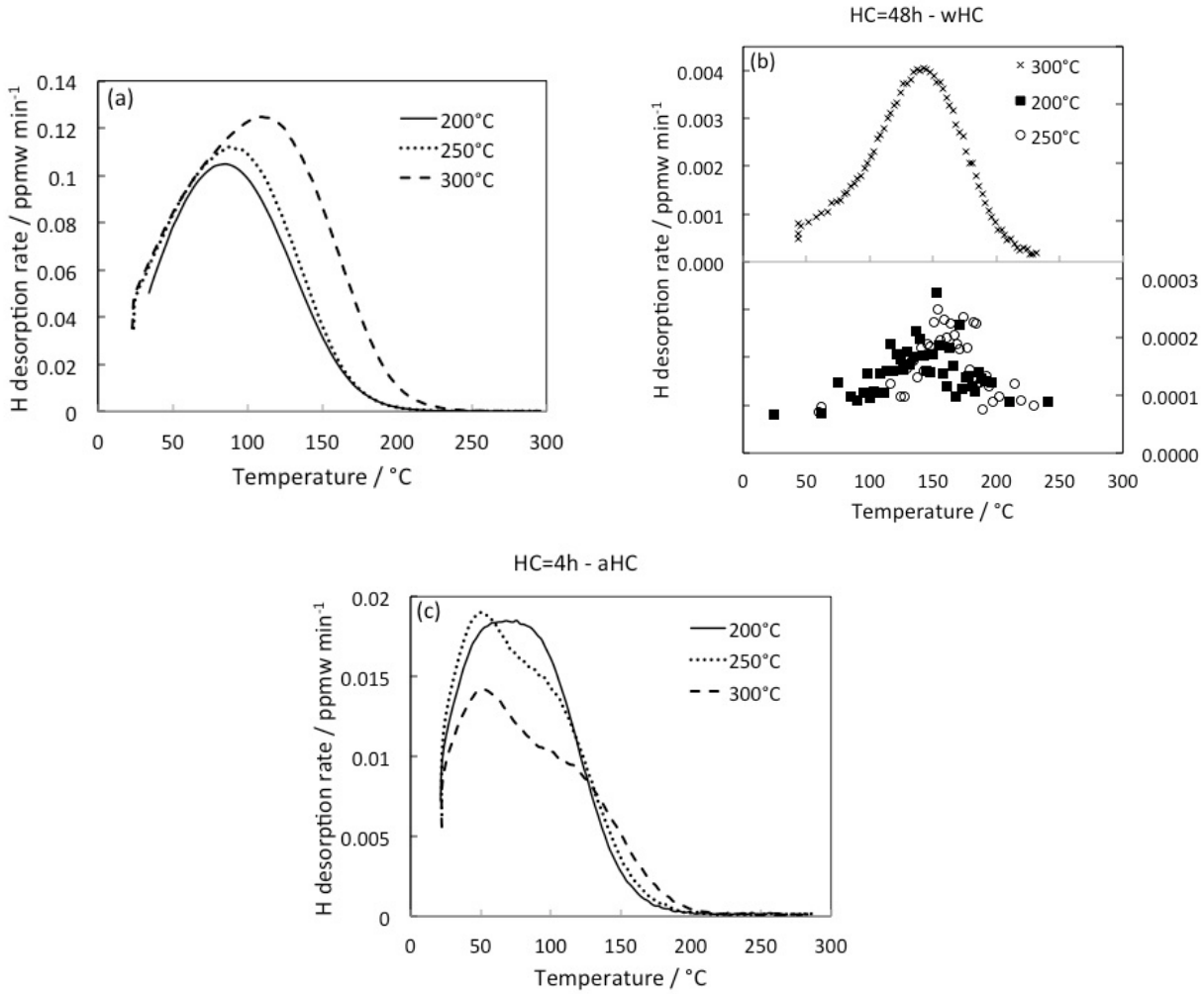

Fig. 3- Thermal desorption analysis for samples charged with hydrogen for: (a) 48 h and TDA 15 minutes after H-charging (HC=48h – aHC); (b) 48 h and TDA one week after H-charging (HC=48h – wHC) and (c) 4 h and TDA 15 minutes after H-charging (HC=4h – aHC). ppmw refers to parts per million by weight.

Table 3. TDA data. H_T is the total hydrogen desorbed, and $T_{1,peak}$ and $T_{2,peak}$ are the first and second peak temperatures, respectively.

Transformation temperature	HC = 48h - aHC		HC = 48h - wHC		HC = 4h - aHC		
	H_T/ppmw	T_{peak}/°C	H_T/ppmw	T_{peak}/°C	H_T/ppmw	$T_{1,peak}$/°C	$T_{2,peak}$/°C
200 °C	11.27	82.8	0.09	150	2.14	70.0	---
250 °C	13.08	86.9	0.10	150	2.14	50.4	90
300 °C	17.46	112.0	0.48	150	1.75	50.4	98

In the unsaturated condition (samples charged with hydrogen for 4 h and analysed 15 minutes after H-charging), hydrogen desorption effectively occurred in two stages (Figure 3c). The amount of hydrogen absorbed during charging decreased as the volume fraction of retained austenite increased (Table 3). At isothermal transformation temperatures of 250 °C and 300 °C it was possible to determine two peak temperatures. The first peak is associated with hydrogen released from ferrite/austenite interfaces, whereas the second peak temperature

relates to hydrogen in solid solution released from retained austenite. The larger fraction of retained austenite resulted in an increase in second peak temperature.

The effect of volume fraction of retained austenite and surface area of α/γ interfaces on the total amount of hydrogen released is shown in Figure 4. When the fraction of austenite increases, the total hydrogen desorbed increases linearly for hydrogen saturated samples, i.e. the level of hydrogen saturation was found to correlate to the volume fraction of retained austenite rather than to the surface area of α/γ interfaces. The values calculated of the standardized coefficients[1] of S_V (0.46) and V_γ (1.45) using multiple regression prove this result. In the unsaturated condition (samples charged for 4 h), the total hydrogen desorbed decreased when the surface area of α/γ interfaces decreased.

In saturated samples, hydrogen desorption increases with retained austenite volume fraction. In partially charged samples this trend is inversed; the amount of desorbed hydrogen decreases from 2.14 to 1.75 ppmw, for example when the retained austenite fraction increases from 0.26 to 0.34. This is caused by the percolation effect of austenite, which has a threshold value at approximately 0.10 volume fraction [10].

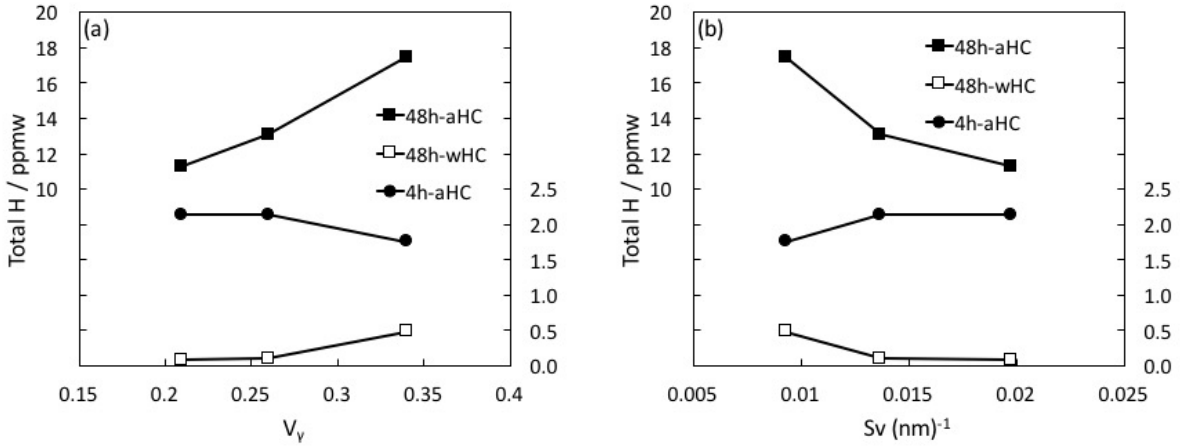

Fig. 4- Total hydrogen desorbed as a function of (a) retained austenite volume fraction (V_γ) and (b) surface area of ferrite-retained austenite (S_V).

Discussion

In TDA, the measured quantity is the rate desorption of hydrogen that diffuses out through the material undergoing trapping and detrapping processes. It was showed (Table 3) that about 97-99 % of the total hydrogen absorbed by the samples is released at room temperature when TDA is carried out one week after H-charging. This hydrogen is diffusible or weakly trapped (reversibly trapped hydrogen). When trapping is weak, thermally activated diffusion through lattice is the rate-determining process of desorption during the temperature ramp and the local equilibrium exists between the lattice and trapped hydrogen, i.e., the rates of trapping and detrapping are equal. In this work, the heating rate of 50 °C/h during TDA ensures local equilibrium at each step of the slow temperature increase and dynamic local equilibrium between the hydrogen in the trap sites and lattice sites.

[1] Standardized coefficients enable to compare the relative effects of two or more variables that have different units of measurement by converting the variables into standard deviation units.

The effect of hydrogen trapping in retained austenite, at α/γ interfaces and dislocations during TDA experiments was simulated by using the hydrogen desorption models developed by Song et al. [20]. This model permits multiple traps to be included in the analysis and the consequence of the initial charging stage is to distribute the hydrogen across the lattice and trap sites assuming local equilibrium. The authors assume one-dimensional diffusion occurring through the lattice in a direction normal to the plane drawn by the free surface of a steel sheet using a finite difference method (FDM), while the hydrogen interacts with multiple kinds of traps of different binding energies, such as interfaces, dislocations, and retained austenite [20].

For the local equilibrium condition, Oriani's equation was used [33]:

$$\frac{\theta_t(1-\theta_L)}{\theta_L(1-\theta_t)} = \exp\left(\frac{E_b}{RT}\right) \quad [1]$$

where θ is the fractional occupancy of trap (t) or lattice (L) sites (θ=C/N), C is the hydrogen concentration in trap (t) or lattice (L) sites, N is the number of trap (t) or lattice (L) sites per m^3, T is the absolute temperature and E_b is the trap binding energy (J/mol). From Eq. [1], it can be showed that the hydrogen concentration in trap sites is proportional to the number of trap sites.

The hydrogen desorption was simulated considering three traps: dislocations, retained austenite and α/γ interfaces. The number of lattice sites (N_L) in bainitic ferrite, $2.6x10^{29}$ m^{-3}, was calculated as proposed by Song et al. [20]. However, it was assumed in the current model that this value is proportional to the volume fraction of bainitic ferrite. The diffusivity of hydrogen in ferrite considered here was $D_0=5.8x10^{-8}$ m^2s^{-1} and the activation energy, Q=4.5 kJ/mol [34]. The number of trap sites at α/γ interfaces, Nt_1, was assumed proportional to the surface area per unit volume and dislocation density [35]. The number of trap sites in the retained austenite, Nt_2, was assumed proportional to the volume fraction of retained austenite. The number of trap site at dislocations was assumed to be $Nt_3=\pi.\rho.b^2.N_L$, where b is the magnitude of the dislocation Burges vector ($2.7x10^{-10}$ m), ρ is the dislocation density and N_L is the number of lattice sites.

Peet and Hojo [7] have conducted thermal desorption experiments in nanostructured bainitic steels, including one tempered at 500 °C. In the sample as-isothermally transformed with 35.1% retained austenite the amount of hydrogen desorbed was 7.1 ppmw, but in the tempered sample (without retained austenite) the amount of hydrogen desorbed was 3.0 ppmw. The amount of hydrogen in ferrite (stored at interfaces and dislocations) was 3.0 ppmw (the cementite itself is not a prominent trap in tempered structures [36]) and 4.1 ppmw in retained austenite.

Considering this result, it was assumed in the current model that the same number of trap sites at α/γ interfaces and in retained austenite for samples isothermal transformed at 200 °C, charged with hydrogen for 48 h, and analysed by TDA 15 minutes after H-charging. The number of trap sites at dislocations, assuming $\rho=7x10^{15}$ m^{-2} for nanostructured bainite transformed at 200 °C (according to Garcia-Mateo et al. [23]) is $Nt_3=3x10^{26}$ m^{-3}, and the trap binding energy for dislocations associated with the elastic strain field is 27 kJ mol^{-1} [19]. Using these conditions in the model, the amount of hydrogen desorbed from dislocations, interfaces and retained austenite was 0.7, 5.0 and 6.3 ppmw respectively. After aging for 15 min the amount of H left in the sample at dislocations is 6% the total absorbed amount. The H atoms that were weakly trapped at dislocations would have been released from the

sample during this aging period. If the transformation temperature increases, ~~as~~ the dislocation density decreases, and the number of trap sites at dislocations is reduced. Therefore, the amount of H left in the sample at dislocations is negligible for samples transformed at 250 and 300 °C.

Therefore, no separate peak related to this trap must be present in the spectrum, and in this work the hydrogen desorption was simulated considering only two traps: retained austenite and α/γ interfaces.

The hydrogen saturated samples were investigated first. The number of trap sites and the trap binding energies for α/γ interfaces and retained austenite were obtained by fitting the numerical model to the TDA curves for samples isothermal transformed at 200 °C, and analysed 15 minutes after H-charging. The thermal desorption rates were simulated assuming the following conditions: charging time of 48 h and the room temperature release time of 15 minutes. The number of trap sites obtained was 3.6×10^{25} m^{-3} and the trap binding energies were determined using the simulation as 42 and 47 kJ/mol for α/γ interfaces and retained austenite respectively. These energy values were used to model the TDA curves for samples isothermally transformed at 250 °C and 300 °C, using the values of the number of trap sites given in Table 4. The closest fit to the data under the assumptions of unidirectional hydrogen flow, local equilibrium, and the two kinds of traps used is presented in Figure 5a. The amount of hydrogen desorbed from ferrite (interfaces and dislocations) and retained austenite derived from simulation is given in Table 4. The small difference in the binding energies of the two kinds of traps leads to overlap of the detrapping events from the two traps and hence an apparently simple peak shape.

Table 4. Parameters used in the modelling of TDA curves of saturated samples with hydrogen. N_L is a number of lattice sites, Nt_1 and Nt_2 are the number of trap sites at interfaces and retained austenite respectively. Hα and Hγ are the amount of hydrogen desorbed in ferrite and retained austenite respectively as derived from the simulation.

Transformation temperature	V_γ	$Sv/(nm)^{-1}$	N_L/m^{-3}	Nt_1/m^{-3}	Nt_2/m^{-3}	Hα/ppmw	Hγ/ppmw
200 °C	0.21	0.01975	2.01×10^{29}	3.6×10^{25}	3.6×10^{25}	5.0	6.3
250 °C	0.26	0.01370	1.89×10^{29}	2.7×10^{25}	5.4×10^{25}	3.6	9.5
300 °C	0.34	0.00930	1.68×10^{29}	2.1×10^{25}	7.0×10^{25}	3.3	14.1

In the modelling of the TDA curves of hydrogen unsaturated samples analysed 15 minutes after H-charging, and the following conditions were assumed: charging time of 4 h and the room temperature release time of 15 minutes. The trap binding energies were estimated at 42-44 kJ/mol and 52 kJ/mol for α/γ interfaces and retained austenite respectively. The closest fit to the data is presented in Figure 5b. For the conditions studied, a relatively larger difference in the binding energies of the two kinds of traps leads to a curve in which hydrogen evolution effectively occurs in two stages. The trap binding energy for retained austenite is larger than the value of 47 kJ/mol determined for saturated samples analysed 15 minutes after H-charging. In case of unsaturated samples the traps with higher binding energy along the distribution are filled first, and this explain the higher trap binding energy in these samples. The trap binding energy has a distribution around an average binding energy for each trap site.

The trap binding energy of 52 kJ/mol is closely related to the peak temperature of 150 °C for hydrogen saturated samples analysed one week after H-charging.

The trap binding energies ranging from 47-52 kJ/mol for retained austenite are nearly equal to the values reported by Ningshen et al. [37] and Park et al. [38]. The trap binding energies estimated by Ningshen et al. varied from 44.2 to 51.9 kJ/mol, depending on the austenitic alloy used. Park et al. [38] reported a trap binding energy for retained austenite of 55 kJ/mol. These trap binding energies estimated from thermal analysis are nearly equal to the activation energy for hydrogen diffusion in austenitic matrix (48-54 kJ/mol) [32]. The binding energy obtained in this work suggests that the observed hydrogen trapping capacity mostly originates from austenite lattice sites for samples heated up to 300 °C.

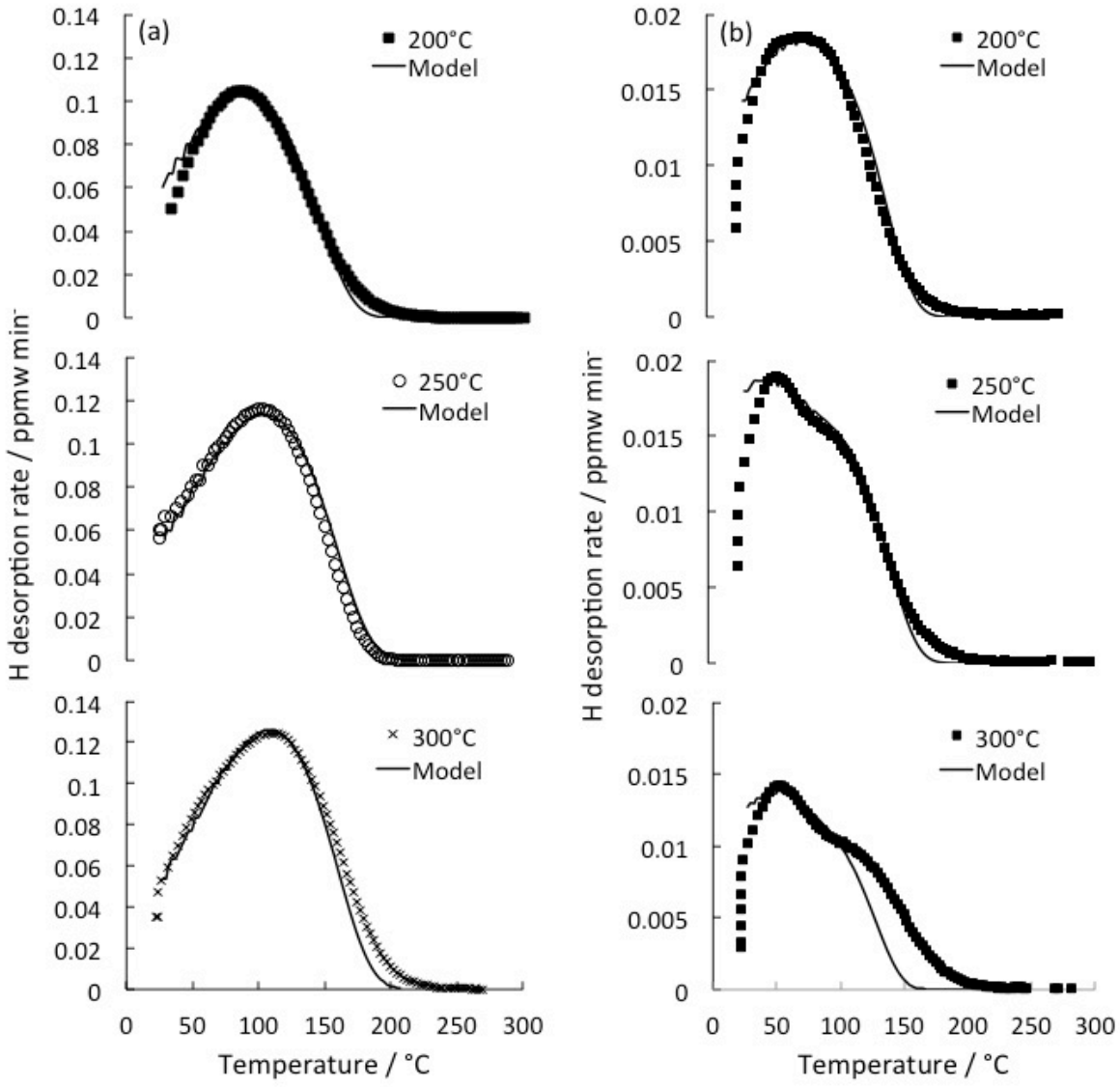

Fig. 5- Comparison between experimental and simulated hydrogen desorption curves for: (a) saturated samples analysed after 15 minutes and (b) samples charged for 4 h analysed 15 minutes after H-charging.

The numerical analysis was used to explore the effect of the α/γ interfaces and retained austenite as the preferred location for hydrogen trapping, considering saturated samples. The parameters used were: 1) trap binding energy of 42 and 47

kJ/mol for interfaces and retained austenite; 2) number of trap sites at interfaces $Nt_1(Sv_1)=3.6x10^{25}$ m^{-3} and $Nt_1(Sv_2)=0.62xNt_1(Sv_1)$; 3) number of trap sites in retained austenite $Nt_2(V\gamma_1)=3.6x10^{25}$ m^{-3} and $Nt_2(V\gamma_1)=0.62xNt_2(V\gamma_2)$; 4) charging time of 48 h and the room temperature release time of 15 minutes.

The results show that for the same volume fraction of retained austenite, an increase of 62 % surface area per unit volume implied in an increase of hydrogen desorbed by about 29 %. For the same surface area per unit volume of interfaces an increase of 62 % in retained austenite fraction represented an increase of hydrogen desorbed by about 36% (Figure 6). The retained austenite is more effective in trapping hydrogen than ferrite-retained austenite interfaces. This result is supported by the close correlation between the total hydrogen content after saturation and the volume fraction of retained austenite (Figure 4) rather than surface area of α/γ interfaces. In the unsaturated condition, the retained austenite becomes more effective in hindering the infusion of hydrogen into nanostructured bainite than the α/γ interfaces (Figure 4).

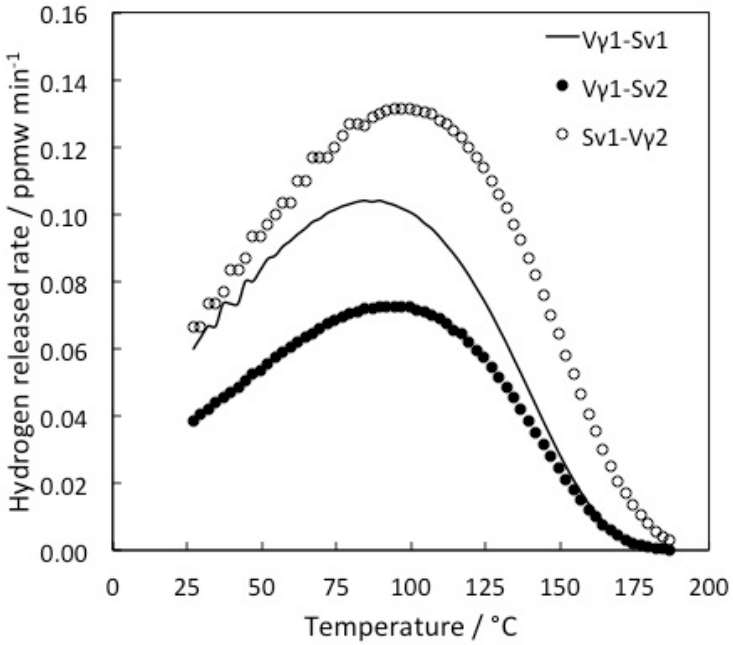

Fig. 6- Simulated hydrogen desorption curves as a function of surface area of α/γ interfaces and volume fraction of retained austenite.

It was observed, in unsaturation condition, that the retained austenite is effective in reducing the intake of hydrogen, and so, it may be expected that this phase will aid in resisting to the infusion of hydrogen in service conditions.

Conclusions

The results presented in this work have demonstrated, by using thermal desorption analysis, the potency of α/γ interfaces and retained austenite as hydrogen trapping sites in nanostructured bainitic steel.

The retained austenite is more effective in trapping hydrogen than ferrite-retained austenite interfaces, since a good correlation between the total hydrogen content analysed just after saturation and the volume fraction of retained austenite was observed, rather than ~~the~~ surface area of α/γ interfaces. In the unsaturated

condition, the retained austenite is effective at hindering the infusion of hydrogen into nanostructured bainite.

It was observed that 97-99% of the total hydrogen absorbed was released after one week at room temperature and that the hydrogen atoms that remain in films and micro blocks of retained austenite were released at a high peak temperature (≈150 °C).

A model assuming local equilibrium was able to reproduce the hydrogen desorption behaviour of the saturated and unsaturated samples with hydrogen by taking into consideration the effect of two trap binding energies, and retained austenite and ferrite-retained austenite interfaces as traps. A trap binding energy ranging from 47-52 kJ/mol was estimated for retained austenite and this value suggests that the observed hydrogen trapping capacity is mostly provided by the austenite lattice sites.

Acknowledgements

The work was supported in part by a grant from Conselho Nacional de Desenvolvimento Científico e Tecnológico, Brazil.

References

[1] H.K.D.H. Bhadeshia, The first bulk nanostructured metal, Sci. Technol. Adv. Mater. 14 (2013) 1-7.

[2] C. Garcia-Mateo, F.G. Caballero and H.K.D.H. Bhadeshia, Acceleration of Low-temperature Bainite, ISIJ Int. 43 (2003) 1821–1825.

[3] H.K.D.H. Bhadeshia, Nanostructured bainite, Proc. Royal Soc. Lond. A 466 (2010) 3–18.

[4] K.H. So, J.S. Kim, Y.S. Chun, K.T. Park, Y.K. Lee and C.S. Lee, Hydrogen Delayed Fracture Properties and Internal Hydrogen Behavior of a Fe–18Mn–1.5Al–0.6C TWIP Steel, ISIJ Int. 49 (2009) 1952-1959.

[5] M. Zhang, M. Wang and H. Dong, Hydrogen absorption and desorption during heat treatment of AISI 4140 Steel, J. Iron Steel Res. Int. 21 (2014) 951-955.

[6] A. Oudriss, A. Fleurentin, G. Courlit, E. Conforto, C. Berziou, C. Rébéré, S. Cohendoz, J. M. Sobrino, J. Creus and X. Feaugas, Consequence of the diffusive hydrogen contents on tensile properties of martensitic steel during the desorption at room temperature, Mater. Sci. Eng. A 598A (2014) 420–428.

[7] M. J. Peet and T. Hojo, Hydrogen susceptibility of nanostructured bainitic steels, Metall. Mater. Trans. A 36A (2016) 718-725.

[8] H. K. D. H. Bhadeshia, Prevention of hydrogen embrittlement in steels, ISIJ Int. 56 (2016) 24–36.

[9] R. A. Oriani, The physical and metallurgical aspects of hydrogen in metals, In ICCF4, Fourth International Conference on Cold Fusion, 1993, Palo Alto, CA 94304.

[10] L. C. D. Fielding, E. J. Song, D. K. Han, H. K. D. H. Bhadeshia and D. W. Suh, Hydrogen diffusion and the percolation of austenite in nanostructured bainitic steel, Proc. Royal Soc. Lond. A 70 (2014) 20140108 (18pp).

[11] D. Figueroa and M. J. Robinson, The effects of sacrificial coatings on hydrogen embrittlement and re-embrittlement of ultra-high strength steels, Corros. Sci. 50 (2008) 1066-1079.

[12] K. I. Sugimoto, Fracture strength and toughness of ultra-high strength TRIP aided steels, Mater. Sci. Technol. 25 (2009) 1108-1117.

[13] M. Wang, C. C. Tasan, M. Koyama, D. Ponge and D. Raabe, Enhancing hydrogen embrittlement resistance of lath martensite by introducing nano-films of interlath austenite, Metall. Mater. Trans. A 46A (2015) 3797-3802.
[14] H. K. D. H. Bhadeshia and D. V. Edmonds, The bainite transformation in a silicon steel, Metall. Trans. A 10 (1979) 895-907.
[15] J. Cornide, G. Miyamoto, F. G. Caballero, T. Furuhara, M. K. Miller and C. García-Mateo, Distribution of dislocations in nanostructured bainite, Solid State Phenom. 172-174 (2011) 117-122.
[16] F. G. Caballero, H. W. Yen, M. K. Miller, J. R. Yang, J. Cornide and C. Garcia-Mateo, Complementary use of transmission electron microscopy and atom probe tomography for the examination of plastic accommodation in nanocrystalline bainitic steels, Acta Mater. 59 (2011) 6117-6123.
[17] E. Pereloma, H. Beladi, L. Zhang and I. Timokhina, Understanding the Behavior of Advanced High-Strength Steels Using Atom Probe Tomography, Metall. Mater. Trans. A 43A (2012) 3958-3971.
[18] C. Garcia-Mateo, F. G. Caballero, T. Sourmail, J. Cornide, V. Smanio and R. Elvira, Composition design of nanocrystalline bainitic steels by diffusionless solid reaction, Met. Mater. Int. 20 (2014) 405-415.
[19] W. Y. Choo and J. Y. Lee, Hydrogen trapping phenomena in carbon steel, J. Mater. Sci. 17 (1982) 1930–1938.
[20] E. J. Song, D. W. Suh and H. K. D. H. Bhadeshia, Theory for hydrogen desorption in ferritic steel, Comput. Mater. Sci. 79 (2013) 36-44.
[21] B. A. Szost, R. H. Vegter and P. E. J. Rivera-Díaz-Del-Castilho, Hydrogen-trapping mechanisms in nanostructured steels, Metall. Mater. Trans. A 44A (2013) 4542-50.
[22] J. H. Ryu, Y. S. Chun, C. S. Lee, H. K. D. H. Bhadeshia and D. W. Suh, Effect of deformation on hydrogen trapping and effusion in TRIP-assisted steel, Acta Mater. 60 (2012) 4085–92.
[23] C. Garcia-Mateo, F. G. Caballero, C. Capdevila and C. G. de Andres, Estimation of dislocation density in bainitic microstructures using high-resolution dilatometry, Scr. Mater. 61 (2009) 855–858.
[24] L. C. Chang and H. K. D. H. Bhadeshia, Austenite films in bainitic microstructures, Mater. Sci. Technol. 11 (1995) 874–881.
[25] W. Solano-Alvarez and H. K. D. H. Bhadeshia, White-etching matter in bearing steel. Part I: controlled cracking of 52100 steel, Metall. Mater. Trans. A 45A (2014) 4916-4931.
[26] D. J. Dyson and B. Holmes, Effect of alloying additions on the lattice parameter of austenite, J. Iron Steel Res. Int. 208 (1970) 469–474.
[27] E. Honda and Z. Nishiyama, Nature of the Tetragonal and Cubic Martensites, Trans. Am. Soc. Steel Treat. 20 (1932) 464-470.
[28] H. K. D. H. Bhadeshia, S. A. David, J. M. Vitek and R. W. Reed, Stress induced transformation to bainite in Fe-Cr-Mo-C pressure vessel steel, Mater. Sci. Technol. 7 (1991) 686-98.
[29] F. G. Caballero, M. K. Miller, C. Garcia-Mateo and J. Cornide, New experimenta levidence of the diffusionless transformation nature of bainite, J. Alloys Compd. 577S (2013) S626–S630.
[30] B. Avishan, C. Garcia-Mateo, S. Yazdania and F. G. Caballero, Retained austenite thermal stability in a nanostructured bainitic steel, Mater. Charact. 81 (2013) 105-10.

[31] B. Avishan, S. Yazdani, F. G. Caballero, T. S. Wang and C. Garcia-Mateo, Characterisation of microstructure and mechanical properties in two different nanostructured bainitic steels, Mater. Sci. Technol. 31 (2015) 1508-20.
[32] S. Xiukui, X. Jian and L. Yiyi, Hydrogen permeation behaviour in austenitic stainless steels, Mater. Sci. Eng. A 114 (1989) 179–187.
[33] R.A. Oriani, The diffusion and trapping of hydrogen in steel, Acta Metall. 18 (1970) 147-57.
[34] H. Hagi and Y. Hayashi, Effect of dislocation trapping on hydrogen and deuterium diffusion in iron, Trans. JIM. 28 (1987) 368–74.
[35] K. Ono and M. Meshii, Hydrogen detrapping from grain boundaries and dislocations in high purity iron, Acta Metall. Mater. 40 (1992) 1357–64.
[36] B. D. Craig, On the elastic interaction of hydrogen with precipitates in lath martensite, Acta Metall. 25 (1977) 1027–30.
[37] S. Ningshen, M. Uhlemann, F. Schneider and H. Khatak, Diffusion behaviour of hydrogen in nitrogen containing austenitic alloys, Corros. Sci. 43 (2001) 2255-64.
[38] Y. Park, I. Maroef, A. Landau and D. Olson, Retained austenite as a hydrogen trap in steel welds, Weld. Res. (2002) 27-35.

Materials Characterization 134 (2017) 96-102